

# SECULAR AND SEMI-NONSECULAR MODELS OF CROSS-POLARIZATION KINETICS FOR REMOTE SPINS: AN APPLICATION FOR NANO-STRUCTURED CALCIUM HYDROXYAPATITE

V. Klimavičius<sup>a,b</sup>, F. Kuliešius<sup>a</sup>, E. Orentas<sup>b</sup>, and V. Balevičius<sup>a</sup>

<sup>a</sup>*Institute of Chemical Physics, Vilnius University, Saulėtekio 3, 10257 Vilnius, Lithuania*

<sup>b</sup>*Department of Organic Chemistry, Vilnius University, Naugarduko 24, 03225 Vilnius, Lithuania*

Email: vytautas.balevicius@ff.vu.lt

Received 15 January 2021; revised 18 February 2021; accepted 19 February 2021

The  $^1\text{H} \rightarrow ^{31}\text{P}$  cross-polarization (CP) kinetics in the nanostructured calcium hydroxyapatite (nano-CaHA) was measured under moderate (5 kHz) magic-angle spinning (MAS) rate. This material was chosen as it contains the distanced  $^1\text{H}$ - $^{31}\text{P}$  spin pairs and the interactions between them are characterized by a relatively low dipolar coupling ( $b$ ) that could be comparable with the spin-diffusion rates ( $R$ ). Therefore, the physical legitimacy to use the secular solution of the quantum Liouville–von Neumann equation is doubtful. The semi-nonsecular model of spin dynamics was applied, and the results were compared with those obtained by the secular approach. The comparable results obtained by both models show that the secular model is applicable, with certain reservation, also in the case of  $|b| \approx R$ . The extremely high anisotropy of spin diffusion in the nano-CaHA was deduced. This can be a matter of the applied approach, as the interactions of the  $^{31}\text{P}$  spins with the proton bath were neglected in both models. The high anisotropy could also be caused by the physical reasons that stem from the structural and proton diffusion features of CaHA. This material belongs to low-dimensional proton conductors possessing a large motional freedom for protons along  $\text{OH}^-$  chains.

**Keywords:** solid-state NMR, cross-polarization, spin diffusion, magic-angle spinning, calcium hydroxyapatite

## 1. Introduction

Bone tissue consists of about 70% of calcium phosphates (CaPs) that make CaPs materials of choice for potential treating of bone diseases by repairing damaged bone tissues. For the successful application in medicine, the process of CaP biomineralization and the interaction between CaPs and biological environment needs to be understood [1]. Hydroxyapatites (HAs) are thermodynamically the most stable form of CaPs, and therefore HAs are widely applied in implantology, orthopedic and periodontal surgery [2, 3]. Each particular application depends on HA structure, crystallinity,

particles size and morphology [4]. Calcium hydroxyapatite ( $\text{Ca}_{10}(\text{PO}_4)_6(\text{OH})_2$ , CaHA) represents a privileged member for the above applications due to its close resemblance to the mineral of hard tissues (bone, enamel, dentin, etc.) resulting in high biocompatibility [5].

CaHA is an attractive object for investigation from the physical point of view. It belongs to the class of low-dimensional proton-conducting materials possessing a motional freedom for protons along  $\text{OH}^-$  chains [6, 7]. An interplay of the surface and bulk effects may further result in other interesting features of the nanostructured CaHA (nano-CaHA) [8].

Cross-polarization (CP), combined with magic-angle spinning (MAS), is one of the ‘classical’ and most widely used methods in solid-state NMR spectroscopy [9–11]. CP is a powerful tool for studying fine structural details and dynamics in complex materials [12–14]. The processing of CP kinetic data, i.e. the consideration of the evolution of interactions between spins in time (contact time) provides the rates of spin diffusion and spin–lattice relaxation, the profiles of distribution of dipolar coupling and some other parameters characterizing the effective sizes of spin clusters [15–17].

In the present work, the comparative study of application of secular and semi-nonsecular spin dynamics models for experimental CP MAS kinetics was conducted. To this end, the  $^1\text{H} \rightarrow ^{31}\text{P}$  CP MAS kinetics under moderate MAS rate (5 kHz) was measured. Nano-CaHA contains the distanced  $^1\text{H}$ – $^{31}\text{P}$  spin pairs and the interactions between them are characterized by the relatively low dipolar coupling constant values that could be compared with the spin-diffusion rates. The earlier studies [15, 16] have revealed that the nano-CaHA is a slowly relaxing spin system. This makes the nano-CaHA very suitable for testing various microscopic quantum models of spin dynamics without taking into account the spin–lattice relaxation effects.

## 2. Experiment

The nano-CaHA was obtained from *Aldrich* (synthetic, 99.999%, from metal basis). The material was characterized by scanning electron microscopy (SEM) and energy-dispersive X-ray analysis (EDX), for details see [16]. In order to remove the adsorbed water, the sample was vacuum-dried at 373 K for four days.

The solid-state NMR experiments were performed using an 600 MHz *Bruker* AVANCE NEO NMR spectrometer equipped with a 2.5 mm *Bruker* TriGamma triple resonance MAS probe. The experiments were performed in 14.095 T magnetic field using an *Ascend* 54 mm standard-bore superconducting magnet. The resonance frequencies of  $^1\text{H}$  and  $^{31}\text{P}$  nuclei were 600.3 and 243.0 MHz, respectively. The  $^1\text{H} \rightarrow ^{31}\text{P}$  CP MAS experiments were performed for the spinning sample at 5 kHz at the  $n = +1$  Hartmann–Hahn (HH) matching condition. The CP contact was achieved with rectangular 71 and 76 kHz RF pulses for  $^{31}\text{P}$  and  $^1\text{H}$ , re-

spectively. The sample temperature was set to 298 K and controlled by a *Bruker* BCU II temperature regulation system. Spectra consisted of 7142 real data points and were registered using a single scan, the repetition delay was set to 125 s, that is equal to  $5 \cdot T_1$  (the spin–lattice relaxation time). The CP MAS kinetics were registered by varying the contact times from 50  $\mu\text{s}$  to 10 ms in increments of 10  $\mu\text{s}$ . Processing of CP MAS kinetics was carried out using the Microcal Origin 9 and MathCad 15.0 packages.

## 3. Theoretical models of CP kinetics

The most widely used theoretical model that exhibits the coherent oscillatory behaviour of CP intensity originates from the work of Müller et al. [18], the so-called I–I\*–S model [11, 12, 19]. The system is treated as a strongly coupled I\*–S spin pair (I =  $^1\text{H}$  and S =  $^{31}\text{P}$  spins in the present work) immersed in a spin bath consisting of the remaining I spins. The model assumes that only one spin I\* interacts with the I-spin bath or infinite energy reservoir of I spins, that is described in a phenomenological way. The kinetics of the CP signal intensity  $I(t)$  is then expressed as

$$I(t) = I_0 \left[ 1 - \frac{1}{2} e^{-k_1 t} - \frac{1}{2} e^{-k_2 t} \cos\left(\frac{b}{2} t\right) \right], \quad (1)$$

where the parameters  $k_1$  and  $k_2$  are the spin-diffusion rate constants. The cosine-oscillation frequency is  $b/2$ , i.e.  $\frac{1}{2}$  of the dipolar splitting, that depends on the gyromagnetic ratios ( $\gamma_I, \gamma_S$ ) of two interacting nuclei (I and S), the distance  $r$  between them and the angle  $\theta$  between the  $\mathbf{r}$  vector and the magnetic field:

$$b = \frac{\gamma_I \gamma_S \hbar}{r^3} \frac{(3 \cos^2 \theta - 1)}{2}. \quad (2)$$

Later on, the model was modified by Naito and McDowell [20] introducing the spin–lattice relaxation rate of spin I in the rotating frame ( $1/T_{1\rho}$ ) and the anisotropy of spin diffusion. Recently, the I–I\*–S model and spin-diffusion properties were revised very thoroughly by Hirschinger and Raya by solving the quantum mechanical master equation using various approaches and the formalism of spin-diffusion superoperators [12, 19, 21]. For a fast

fluctuating I-spin bath, the spin-diffusion super-operator for the reduced density operator  $\hat{\sigma}$  can be written as

$$\begin{aligned} \widehat{\Gamma}(\hat{\sigma}) = & R_{\text{dp}}^I \left[ \hat{I}_z, \left[ \hat{I}_z, \hat{\sigma} \right] \right] + \\ & + R_{\text{df}}^I \left\{ \left[ \hat{I}_x, \left[ \hat{I}_x, \hat{\sigma} \right] \right] + \left[ \hat{I}_y, \left[ \hat{I}_y, \hat{\sigma} \right] \right] \right\} + \\ & + R_{\text{df}}^S \left\{ \left[ \hat{S}_x, \left[ \hat{S}_x, \hat{\sigma} \right] \right] + \left[ \hat{S}_y, \left[ \hat{S}_y, \hat{\sigma} \right] \right] \right\}, \quad (3) \end{aligned}$$

where  $R_{\text{dp}}^I$  and  $R_{\text{df}}^I$  are the (homonuclear) spin-diffusion rate constants of the I\* spin and  $R_{\text{df}}^S$  is that (heteronuclear) of the S spin. The rate constants  $R_{\text{df}}^I$  and  $R_{\text{df}}^S$  are associated with the flip-flop terms of the homonuclear (I–I\*) and heteronuclear (I–S) dipolar Hamiltonians, respectively, and allow the complete thermal equilibration with the bath, whereas  $R_{\text{dp}}^I$  acts on the damping of the coherence driving the system to the internal quasi-equilibrium [21].

The usual approximation considers that the I–S interaction with environment is neglected, and thus the rate constant of the heteronuclear spin diffusion of the S spin is set as  $R_{\text{df}}^S = 0$ . In this case, the spin-diffusion rate constants  $k_1$  and  $k_2$  are related with  $R_{\text{dp}}^I$  and  $R_{\text{df}}^I$  as  $k_1 = R_{\text{df}}^I + R_{\text{dp}}^I/2$  and  $k_2 = R_{\text{df}}^I$  and Eq. (1) can be rewritten as

$$I(t) = I_0 \left[ 1 - \frac{1}{2} e^{-R_{\text{df}}^I t} - \frac{1}{2} e^{-(R_{\text{df}}^I + R_{\text{dp}}^I/2)t} \cos\left(\frac{b}{2}t\right) \right]. \quad (4)$$

Equations (1) and (4) are valid at the Hartmann–Hahn condition only if two secular approximations are satisfied: (i) the applied RF fields are much stronger than the I–S coupling ( $\omega_{\text{I}^*}, \omega_{\text{S}} \gg |b|$ ); (ii) the I–S coupling constant is much larger than the spin-diffusion rate constants ( $|b| \gg R_{\text{df}}^I, R_{\text{dp}}^I$ ). Therefore, the physical legitimacy to use Eqs. (1) and (4) for describing the distanced, and thus weakly interacting spins ( $b \approx R_{\text{df}}^I, R_{\text{dp}}^I$  or even less) is in a certain doubt. Note that Alvarez et al. [22] have obtained the analytical nonsecular solution of the master (Liouville–von Neumann) equation for arbitrary values of the homonuclear spin-diffusion rate constants, however, for a static sample (no MAS) and neglecting the I–S interaction with environment ( $R_{\text{df}}^S = 0$ ). Nevertheless, the complete expression of the general nonsecular equation is

rather cumbersome to implement. In Ref. [21] it was shown that the generalized Liouville–von Neumann quantum mechanical equation has a semi-nonsecular analytical solution when  $|b| \gg |R_{\text{df}}^I - R_{\text{df}}^S|$

$$\begin{aligned} I(t) = & I_0 \left[ 1 - \frac{1}{2} e^{-R_{\text{df}}^I t} \left\{ 1 + \right. \right. \\ & \left. \left. + e^{\frac{1}{2} R_{\text{dp}}^I t} \left[ \cosh(\varphi t) + \frac{R_{\text{dp}}^I}{2\varphi} \sinh(\varphi t) \right] \right\} \right], \quad (5) \end{aligned}$$

where

$$\varphi = \sqrt{\left(R_{\text{dp}}^I/2\right)^2 - b^2}. \quad (6)$$

From Eqs. (5) and (6) it is easy to see that transient oscillations of CP intensity will appear when  $\varphi$  becomes imaginary, i.e.  $b^2 > (R_{\text{dp}}^I/2)^2$ . If  $(R_{\text{dp}}^I/2)^2 > b^2$ , oscillations convert to an overdamped regime.

Both the secular (Eq. (4)) and semi-nonsecular (Eq. (5)) models were applied processing the experimental CP MAS kinetics data and the results were compared.

#### 4. Results and discussion

As the dipolar splitting  $b$  is an angular function, the proper angular averaging has to be carried out in order to apply Eqs. (4) and (5) to powder samples. For MAS experiments when the HH matching conditions  $\omega_{\text{I}^*} - \omega_{\text{S}} = n\omega_{\text{MAS}}$  are fulfilled for  $n = \pm 1$  (used in the present work)

$$b_{\pm 1} = \frac{D_{\text{IS}}}{2\sqrt{2}} \sin(2\beta), \quad (7)$$

where  $D_{\text{IS}}$  is the heteronuclear I–S dipolar coupling constant ( $D_{\text{IS}} = (1/2\pi) (\mu_0/4\pi) \gamma_I \gamma_S (h/2\pi)/r^3$ , in Hz),  $\beta$  is the polar angle between  $\mathbf{r}$  vector and the MAS rotor axis [23, 24], following [23], the angular averaging (AA) for Eq. (4) is carried out as

$$\cos(bt)_{\text{AA}} = \frac{1}{2} \int_0^\pi \cos(b(\beta)t) \sin(\beta) d\beta, \quad (8)$$

and correspondingly it can be written for the oscillating part  $[\cosh(\varphi t) + \dots \sinh(\varphi t)]$  in Eq. (5). The averaging for Eq. (4) was carried out analytically using the series of Bessel  $J_n$  functions [24, 25] as well as numerically:

$$\cos(bt/2)_{AA} = \begin{cases} J_0\left(\frac{\pi D_{IS}t}{\sqrt{2}}\right) + 2\sum_{k=1}^{\infty} \left[ \frac{1}{1-4(2k)^2} J_{2k}\left(\frac{\pi D_{IS}t}{\sqrt{2}}\right) \right] \\ \text{(Bessel),} \\ \frac{1}{2} \sum_{j=0}^N \cos\left[\frac{\pi D_{IS}t}{\sqrt{2}} \sin\left(\frac{2\pi j}{N}\right)\right] \sin\left(\frac{\pi j}{N}\right) \frac{\pi}{N} \\ \text{(numerical).} \end{cases} \quad (9)$$

In both cases the effects of series truncation ( $\Sigma^{\infty}$ , Bessel) and the increment of discretization ( $\Sigma^N$ , numerical integration) were checked. The results are shown in Fig. 1. The truncation of Bessel series has no significant influence on the precision of calculations due to a very steep suppression ( $\sim 1/(2k)^2$ ) of the contributions from  $J_{2k}(x)$  of higher order. A more delicate situation is encountered when applying the numeri-

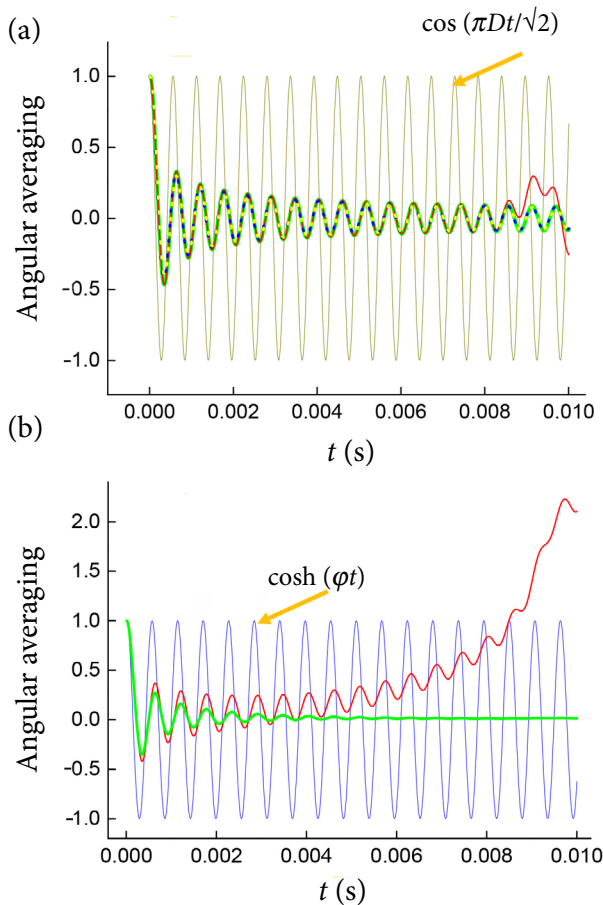


Fig. 1. The angular averaging of CP oscillations for powder samples: (a) secular Eq. 4, using Bessel series: only  $J_0$  is included (yellow dots in coloured online version), the series of  $J_k$  truncated at  $k = 4$  (blue dots online); numerical integration:  $N = 100$  (red line online),  $N = 1000$  (green line online); (b) semi-nonsecular Eqs. 5 and 6,  $N = 100$  (red line online), the same oscillation damped by taking  $R_{dp}^1 = 1000 \text{ s}^{-1}$  (green line online);  $D_{IS} = 5000 \text{ Hz}$  in all cases.

cal method – certain computing artifacts may flash (see the range 8–10 ms in Fig. 1) if the increment of integration is set too rough. This can be checked and mended by optimizing the discretization (e.g. increasing  $N$  in Eq. (9) from 100 to 1000, Fig. 1). Generally speaking, the analytical and the numerical averaging provide practically identical results over the whole range of contact time often used in the kinetic CP MAS experiments. However, the numerical method is more universal, more convenient for programming and can be applied in the cases where the oscillations are described by more complicated (not a single cosine) functions.

The  $^1\text{H} \rightarrow ^{31}\text{P}$  CP MAS kinetics in nano-CaHA were measured and processed using a high density experimental data set (1000 points, Fig. 2). As shown in the earlier works [15–17, 25], this allows one to reduce the excessive freedom in the nonlinear curve fitting targeting its flow towards the ‘true’ minimum on the multi-parameter surface  $\chi^2$ , i.e. to the minimal sum of weighted squares of deviations of the chosen theoretical model curve from the experimental one. This enables one to test and verify a series of multi-parametrical models. The results of fitting are presented in Table 1.

A similar agreement between the theory and the experiment was achieved over the whole contact time range using both models. It is reflected in

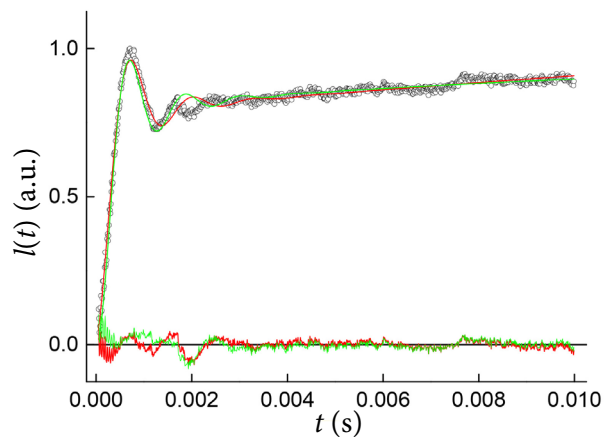


Fig. 2. Experimental  $^1\text{H} \rightarrow ^{31}\text{P}$  CP MAS kinetics data (circles) in nano-CaHA at 5 kHz MAS rate, processed using secular (Eq. (4), red line online, darker) and semi-nonsecular (Eq. (5), green line online, lighter) spin-diffusion models with numerical angular averaging. The fit parameter values are given in Table 1. The regular residuals, i.e. the differences between experimental and theoretically calculated values of CP intensity for both models are shown around  $I(t) = 0$  line.

Table 1. The fit parameters of  $^1\text{H} \rightarrow ^{31}\text{P}$  CP MAS kinetics in nano-CaHA (Fig. 2) obtained using secular and semi-nonsecular models without and with angular averaging (AA).

Model $\Rightarrow$	Secular, Eq. (4)		Semi-nonsecular, Eq. (5)	
	No AA	Numerical AA	No AA	Numerical AA
$R_{\text{dp}}^{\text{I}}, \text{s}^{-1}$	3520	2030	4110	2030
$R_{\text{df}}^{\text{I}}, \text{s}^{-1}$	22	18	19	7
$D_{\text{is}}, \text{Hz}$	1620	2220	2200	2500
$I_0, \text{a.u.}$	1.525	1.564	1.555	1.738
$R^2/\chi^2, \%$	0.976/2.6	0.988/1.8	0.989/1.7	0.986/2.0

the similar statistical parameters  $R^2$  (the correlation coefficient) and  $\chi^2$ . Two most significant discrepancies are noticeable over the whole kinetic curve: (i) high frequency (tens of kHz) oscillations of weak intensity at very short contact times ( $<1$  ms) and (ii) the non-random residuals close to 2 ms (Fig. 2). The physical origin of the first one is most likely related with the RF field values, that in principle might be revealed by some additional experiments varying the MAS rate and the settings of HH matching parameters. The second discrepancy might originate from structural features of the nano-CaHA itself. It is known that in pure crystalline CaHA each P atom has two neighbouring protons distanced at 0.385 nm, further two at 0.42 nm, while others are 0.6 nm or more away [26]. The coupling constants  $D_{\text{is}}$  were determined from  $b$  values, rescaling them by a factor of  $\sqrt{2}$  because the HH matching  $n = \pm 1$  was fulfilled in the present experiments.  $D_{\text{is}}$  values of 2200–2500 Hz (Table 1) correspond to P–H distances of 0.267–0.277 nm. Distances of 0.21–0.25 nm are typical of the P–O–H structures that are found in some related systems, such as calcium phosphate gelatin nano-composites [27] or sol-gel derived  $\text{SnO}_2$  nanoparticles capped by phosphonic acids [28]. In CaHA, protons are not part of the phosphate group, and thus such short P...H contacts should not be observed. However, in nano-CaHa the P–O–H structural motifs with P...H distances of 0.20–0.25 nm can be present on the surface layers [29]. Most importantly, the studied models deal with the single dominant P–H couplings between the spins at the shortest distances only, whereas other couplings were not taken into account.

Finally, the extremely high anisotropy of spin diffusion in the nano-CaHA ( $R_{\text{dp}}^{\text{I}}/R_{\text{df}}^{\text{I}} \sim 100\text{--}200$ ), never seen for other studied spin systems, e.g. glycine [17] or some polymers [30, 31], is noteworthy. It can be a matter of the applied models, as the I–S

interaction with environment is neglected in both models ( $R_{\text{df}}^{\text{S}} = 0$ ). On the other hand, the high anisotropy could be caused by the physical reason related with structural and proton diffusion features of CaHA. The long-range proton diffusion pathway in CaHA was evidenced by high-temperature neutron diffraction technique and bond valence method [6]. The proton diffusion via reorientation of hydroxide ions ( $\text{OH}^-$ ) is a complex process resembling a sinusoidal pattern. It consists of one-dimensional proton diffusion pathways along the  $c$  axis in the hexagonal channel and two-dimensional proton migration pathway network on the  $ab$  planes.

## 5. Conclusions

The semi-nonsecular model of spin dynamics has been applied for analysing  $^1\text{H} \rightarrow ^{31}\text{P}$  CP MAS kinetics obtained for the powdered sample under moderate MAS rate. The results have been compared with those obtained by the secular approach.

The comparable results obtained by both models mean that the condition  $|b| \gg R_{\text{df}}^{\text{I}}$  and  $R_{\text{dp}}^{\text{I}}$ , stated as necessary to derive the secular solution of master equation, appeared to be not very crucial. The secular model can be used with certain reservations also in the case of  $|b| \approx R_{\text{dp}}^{\text{I}}$ .

Extremely high anisotropy of spin diffusion ( $R_{\text{dp}}^{\text{I}}/R_{\text{df}}^{\text{I}} \sim 100\text{--}200$ ) in the nano-CaHA is deduced for the first time. This ratio is the same for secular and nonsecular approaches. Probably, it is caused by the spin dynamics in the low-dimensional proton bath in the nano-CaHA.

## Acknowledgements

The authors acknowledge the Center of Spectroscopic Characterization of Materials and Electronic/Molecular Processes (SPECTROVERSUM, www.spectroversum.ff.vu.lt) at the Lithuanian National

Center for Physical Sciences and Technology for the use of spectroscopic equipment. This research is funded by the European Social Fund under Measure No. 09.3.3-LMT-K-712-19-0022 ‘Development of Competences of Scientists, Other Researchers and Students Through Practical Research Activities’. We thank Professor Jérôme Hirschinger (Strasbourg University) for helpful discussion.

## References

- [1] W. Habraken, P. Habibovic, M. Epple, and M. Bohner, Calcium phosphates in biomedical applications: materials for the future? *Mater. Today* **19**, 69–87 (2016).
- [2] R.Z. Le Geros and J.P. Le Geros, in: *Bioceramics and Their Clinical Applications*, ed. T. Kokubo (Woodhead Publishing, Cambridge, 2008) pp. 367–394.
- [3] J.C. Elliott, in: *Reviews in Mineralogy & Geochemistry*, Vol. 48, eds. M.L. Kohn, J. Rakovan, and T.M. Hughes (Mineralogy Society of America, Washington, DC, 2002) pp. 427–453.
- [4] A. Zanotto, M.L. Saladino, D.C. Martino, and E. Caponetti, Influence of temperature on calcium hydroxyapatite nanopowders, *Adv. Nanopart.* **1**, 21–28 (2012).
- [5] *Hydroxyapatite and Related Materials*, eds. P.W. Brown and B. Constantz (CRC Press, 1994).
- [6] M. Yashima, N. Kubo, K. Omoto, H. Fujimori, K. Fujii, and K. Ohoyama, Diffusion path and conduction mechanism of protons in hydroxyapatite, *J. Phys. Chem. C* **118**, 5180–5187 (2014).
- [7] L. Dagys, V. Klimavičius, M. Brodrecht, G. Buntkowsky, and V. Balevicius, Cross-polarization kinetics and fractal nature of thermal equilibration in spin systems: From low-dimensional proton conductors to tripeptides, *J. Phys. Chem. Solids* **152**, 109946(7) (2021).
- [8] M. Ben Osman, S. Diallo-Garcia, V. Herledan, D. Brouri, T. Yoshioka, J. Kubo, Y. Millot, and G. Costentin, Discrimination of surface and bulk structure of crystalline hydroxyapatite nanoparticles by NMR, *J. Phys. Chem. C* **119**, 23008–23020 (2015).
- [9] E.O. Stejskal, J. Schaefer, and J.S. Waugh, Magic-angle spinning and polarization transfer in proton-enhanced NMR, *J. Magn. Reson.* **28**, 105–112 (1977).
- [10] E.O. Stejskal and J.D. Memory, *High Resolution NMR in the Solid State: Fundamentals of CP/MAS* (Oxford University Press, New York, 1994).
- [11] W. Kolodziejski and J. Klinowski, Kinetics of cross-polarization in solid-state NMR: a guide for chemists, *Chem. Rev.* **102**, 613–628 (2002).
- [12] J. Raya, A. Bianco, and J. Hirschinger, Kinetics of  $^1\text{H}$ – $^{13}\text{C}$  multiple-contact cross-polarization as a powerful tool to determine the structure and dynamics of complex materials: application to graphene oxide, *Phys. Chem. Chem. Phys.* **22**, 12209–12227 (2020).
- [13] V. Klimavičius, L. Dagys, V. Chizhik, and V. Balevicius, CP MAS kinetics study of ionic liquids confined in mesoporous silica: Convergence of non-classical and classical spin coupling models, *Appl. Magn. Reson.* **48**, 673–685 (2017).
- [14] S.K. Mann, M.K. Devgan, W.T. Franks, S. Hubbard, C.L. Chan, J. Griffith, D. Pugh, N.J. Brooks, T. Welton, T.N. Pham, et al., MAS NMR investigation of molecular order in an ionic liquid crystal, *J. Phys. Chem. B* **124**, 4975–4988 (2020).
- [15] V. Klimavičius, A. Kareiva, and V. Balevicius, Solid-state NMR study of hydroxyapatite containing amorphous phosphate phase and nanostructured hydroxyapatite: Cut-off averaging of CP MAS kinetics and size profiles of spin clusters, *J. Phys. Chem. C* **118**, 28914–28921 (2014).
- [16] V. Klimavičius, L. Dagys, and V. Balevicius, Subnanoscale order and spin diffusion in complex solids through the processing of cross-polarization kinetics, *J. Phys. Chem. C* **120**, 3542–3549 (2016).
- [17] L. Dagys, V. Klimavičius, T. Gutmann, G. Buntkowsky, and V. Balevicius, Quasi-equilibria and polarization transfer between adjacent and remote spins:  $^1\text{H}$ – $^{13}\text{C}$  CP MAS kinetics in glycine, *J. Phys. Chem. A* **122**, 8938–8947 (2018).
- [18] L. Müller, A. Kumar, T. Baumann, and R.R. Ernst, Transient oscillations in NMR cross-polarization experiments in solids, *Phys. Rev. Lett.* **32**, 1402–1406 (1974).
- [19] J. Raya and J. Hirschinger, Sensitivity enhancement by multiple-contact cross-polarization

- under magic-angle spinning, *J. Magn. Reson.* **281**, 253–271 (2017).
- [20] A. Naito and C.A. McDowell, Anisotropic behavior of the  $^{13}\text{C}$  nuclear spin dynamics in a single crystal of *l*-alanine, *J. Chem. Phys.* **84**, 4181–4186 (1986).
- [21] J. Hirschinger and J. Raya, Analytical descriptions of cross-polarisation dynamics: relaxing the secular approximations, *Mol. Phys.* **113**, 3161–3175 (2015).
- [22] G.A. Alvarez, E.P. Danieli, P.R. Levstein, and H.M. Pastawski, Environmentally induced quantum dynamical phase transition in the spin swapping operation, *J. Chem. Phys.* **124**, 194507(8) (2006).
- [23] S. Hediger, *Improvement of Heteronuclear Polarization Transfer in Solid-State NMR*, Ph. D. Thesis (ETH-Zürich, 1997).
- [24] C.A. Fyfe, A.R. Lewis, and J.M. Chézeau, A comparison of NMR distance determinations in the solid state by cross polarization, REDOR, and TEDOR techniques, *Can. J. Chem.* **77**, 1984–1993 (1999).
- [25] L. Dagys, V. Klimavicius, and V. Balevicius, Processing of CP MAS kinetics: Towards NMR crystallography for complex solids, *J. Chem. Phys.* **145**, 114202(9) (2016).
- [26] W. Kolodziejcki, in: *New Techniques in Solid-State NMR*, ed. J. Klinowski, Vol. 246 (Springer, Berlin, Heidelberg, 2004) pp. 235–270.
- [27] A. Vyalikh, P. Simon, T. Kollmann, R. Kniep, and U. Scheler, Local environment in biomimetic hydroxyapatite–gelatin nanocomposites as probed by NMR spectroscopy, *J. Phys. Chem. C* **115**, 1513–1519 (2011).
- [28] G.P. Holland, R. Sharma, J.O. Agola, S. Amin, V.C. Solomon, P. Singh, D.A. Buttry, and J.L. Yarger, NMR characterization of phosphonic acid capped  $\text{SnO}_2$  nanoparticles, *Chem. Mater.* **19**, 2519–2526 (2007).
- [29] C. Jäger, T. Welzel, W. Meyer-Zaika, and M. Epple, A Solid-state NMR investigation of the structure of nanocrystalline hydroxyapatite, *Magn. Reson. Chem.* **44**, 573–580 (2006).
- [30] L. Dagys, V. Klimkevičius, V. Klimavicius, K. Aidas, R. Makuška, and V. Balevicius, CP MAS kinetics in soft matter: Spin diffusion, local disorder and thermal equilibration in poly(2-hydroxyethyl methacrylate), *Solid State Nuclear Magn. Reson.* **105**, 101641 (2020).
- [31] L. Dagys, V. Klimkevičius, V. Klimavicius, S. Balčiūnas, J. Banys, and V. Balevicius, Cross-polarization with magic-angle spinning kinetics and impedance spectroscopy study of proton mobility, local disorder, and thermal equilibration in hydrogen-bonded poly(methacrylic acid), *J. Polym. Sci.*, **58**, 3253–3263 (2020).

## SEKULIARUSIS IR PUSIAU NESEKULIARUSIS SUKINIŲ KINETIKOS MODELIAI NUTOLUSIEMS SUKINIAMS: TAIKYMAS NANOSTRUKTŪRIZUOTAM KALCIO HIDROKSIAPATITUI

V. Klimavičius<sup>a,b</sup>, F. Kuliešius<sup>a</sup>, E. Orentas<sup>b</sup>, V. Balevičius<sup>a</sup>

<sup>a</sup> *Vilniaus universiteto Cheminės fizikos institutas, Vilnius, Lietuva*

<sup>b</sup> *Vilniaus universiteto Organinės chemijos katedra, Vilnius, Lietuva*

### Santrauka

Ištirta  $^1\text{H} \rightarrow ^{31}\text{P}$  kryžminės poliarizacijos (CP) taikant magiškojo kampo sukimą (MAS) kinetika, vykstanti nanostruktūrizuotame kalcio hidroksiapatite (nano-CaHA). Matavimai atlikti kambario temperatūroje ( $T = 298\text{ K}$ ) sukant bandinį 5 kHz dažniu. Šiai medžiagai yra būdingas didelis protonų mobilumas išilgai  $\text{OH}^- \dots \text{OH}^- \dots$  grandinių. Dėl šios savybės CaHA priskiriamas medžiagų klasei, vadinamajai protonų laidininkei. Eksperimentiniai CP MAS duomenys buvo apdoroti taikant sekuliarųjį ir pusiau nesekuliarųjį sukinių kinetikos modelius. Sekuliarusis apibendrintos kvantinės mechaninės Liouville'o – von Neumann'o lygties sprendinys yra išvedamas išpildant dvi asimptotines sąlygas: 1) pridėtųjų radiolaukų dažniai  $\omega_1$  yra daug didesni už dominuo-

jantį dipolinį I–S (šiam darbe  $I = ^1\text{H}$  ir  $S = ^{31}\text{P}$ ) sukinių sąveikos suskilimą, t. y.  $\omega_{1I}, \omega_{1S} \gg |b|$ ; 2) I–S sąveikos suskilimas yra daug didesnis už sukinių difuzijos spartas ( $|b| \gg R_{dp}^I, R_{dp}^S$ ). Pastaroji sąlyga yra sunkiai išpildoma tokiai nutolusių sukinių sistemai, kokia yra nano-CaHa. Kyla abejonių dėl sekuliarinio modelio taikymo. Gautieji kokybiškai identiški rezultatai byloja, kad CP MAS kinetikos gali būti aprašytos taikant tiek sekuliarųjį, tiek pusiau nesekuliarųjį sukinių kinetikos modelius, netgi tais atvejais, kai  $|b|$  ir  $R_{dp}^I$  yra tos pačios eilės dydžiai. Aptikta anomaliai didelė sukinių difuzijos anizotropija, kuri nepriklauso nuo taikyto modelio. Tai gali būti siejama su žemos dimensijos  $^1\text{H}$  sukinių dinamika nano-CaHA protonų rezervuare.